Published in final edited form as:

Annu Rev Biophys. 2017 May 22; 46: 433–453. doi:10.1146/annurev-biophys-070816-033811.

High-Dimensional Mutant and Modular Thermodynamic Cycles, Molecular Switching, and Free Energy Transduction

Charles W. Carter Jr.

Department of Biochemistry and Biophysics, University of North Carolina at Chapel Hill, Chapel Hill, North Carolina 27514

Abstract

Understanding how distinct parts of proteins produce coordinated behavior has driven and continues to drive advances in protein science and enzymology. However, despite consensus about the conceptual basis for allostery, the idiosyncratic nature of allosteric mechanisms resists general approaches. Computational methods can identify conformational transition states from structural changes, revealing common switching mechanisms that impose multistate behavior. Thermodynamic cycles use factorial perturbations to measure coupling energies between side chains in molecular switches that mediate shear during domain motion. Such cycles have now been complemented by modular cycles that measure energetic coupling between separable domains. For one model system, energetic coupling between domains has been shown to be quantitatively equivalent to that between dynamic side chains. Linkages between domain motion, switching residues, and catalysis make nucleoside triphosphate hydrolysis conditional on domain movement, confirming an essential yet neglected aspect of free energy transduction and suggesting the potential generality of these studies.

Keywords

domain motion; catalysis; tryptophanyl-tRNA synthetase; voltage-gated K channel

INTRODUCTION

> In spite of the extreme diversity of these systems, it may be possible to formulate certain generalizations concerning the functional structures responsible for the regulatory competence of the controlling proteins, allowing them to act as specific mediators….
>
> —Jacques Monod, Jean-Pierre Changeux, and François Jacob (78, p. 306)

The earliest use of the term allosteric described the control of enzymes “by a metabolite acting apparently as a physiological ‘signal’ rather than as a chemically necessary component of the reaction itself” (78, p. 306). In a second paper, Monod et al. (79)

DISCLOSURE STATEMENT

The author is not aware of any affiliations, memberships, funding, or financial holdings that might be perceived as affecting the objectivity of this review.

formulated a two-state molecular model for allosteric enzymes, in particular, the hemoglobin heme–heme interaction. That model implied switching mechanisms, in which alternative packing minima suppress intermediate conformational states, thereby limiting the number of discrete states. Equilibria between discrete states are conceptually important to mechanisms in a wide variety of molecular machines (3–6, 46, 80, 104). To date, however, little has been done to identify coupled side chains, measure their energetic impact on structural equilibria and catalysis (2, 106), or determine how they participate in free energy transduction.

Relevant Previous Reviews

Jencks (57, 59, 61) recognized the challenge of understanding how nucleoside triphosphate (NTP) hydrolysis drives vectorial processes. Astumian (3–5) summarized relationships between conformation and ligand-binding specificity necessary for free energy transduction by diffusive molecular machines. Hilser, Nussinov, and others (46, 80, 85, 104, 107) reviewed the consensus conceptual basis for allostery. The contractility community analyzed the statistical thermodynamic basis for free energy transduction [e.g., Hill and colleagues (31, 49, 50) and Dill and colleagues (27, 43, 89)]. Sweeney and Houdusse (94, 101, 102) detailed the myosin VI cross-bridge cycle, and Vanden-Eijnden and Karplus and colleagues (82, 105) described structural changes responsible for the energetics of rigor to prepower stroke conformational change of the myosin VI converter domain.

Purposes of This Review

The foregoing studies suggest neither how to overcome idiosyncratic mechanistic diversities by systematically identifying the “certain generalizations” of Monod et al. (78) nor how to experimentally map the coupling of ligand-dependent conformational energetics to catalysis of nucleotide triphosphate hydrolysis. Here, I attempt to (*a*) define molecular switches and conformational transition states (60, 61, 109); (*b*) emphasize how higher-dimensional thermodynamic cycles constructed between side chains within modules (96, 109, 111, 112) and between modules (67) connected by molecular switches deepen our understanding of allosteric phenomena; and (*c*) relate long-range coupling to conformational equilibria and catalysis by transducing enzymes (52). A second goal is to introduce experimental studies of the voltage-gated K channel and *Bacillus geostearothermophilus* tryptophanyl-tRNA synthetase (TrpRS) to a wider audience. Experimental coupling energies from the two systems furnish new understanding of free energy transduction mechanisms important in channels, NTP-dependent motors, synthetases, polymerases, and signaling GTPases that exhibit multistate, vectorial behavior (4, 5, 57, 60, 61, 83, 96), enabling them to convert energy sources into work and information (27, 53, 90).

Allostery, Cooperativity, Linkage, and Switching

Discussions of allostery often conflate it with cooperativity and linkage in describing molecular transduction. The terms are not interchangeable and should be distinguished.

Allostery is intramolecular communication—This definition retains the original insight that binding at remote sites induces active-site changes affecting thermodynamic and/or kinetic behavior (78). Newer studies suggest expanding the definition to include more general phenomena that do not require binding remotely. Chemical changes in active-site

ligands produce conformational changes surrounding and remote from the active site and alter the reactivity of remote side chains (42); transducing systems couple such allosteric effects to changes in the affinity for macromolecular partners (31, 50, 74, 75).

Cooperativity implies simultaneous movement—Cooperativity is defined by the sharpness of transitions between different states, achieved by near simultaneous, coordinated movement of different macromolecular components, that is, different active-site residues, packing motifs, separate domains within monomers, or different monomers in an oligomer. Cooperativity implies (*a*) a switching mechanism to suppress intermediate states; (*b*) a conformational transition state, that is, an ensemble in which side chain–side chain interactions assume distinctly higher free energies than they do in either initial or final states; and (*c*) three-dimensional interactions that coordinate simultaneous exchanges of components between states.

Linkage is a metric for free energy—Linkage refers to the strength of energetic coupling between different components whose coordinated movements constitute allosteric communication. Linkage is measured experimentally by perturbing each interacting component (52). Logarithms of rate constants for a thermodynamic cycle of perturbations define coupling free energies in the transition state.

FACTORIAL PERTURBATION AND HIGH-ORDER ENERGETIC COUPLING

Intramolecular energetic coupling implies that free energy sources enforce joint behaviors, enabling higher levels of functionality. Coupling energies arise from unexpected nonadditivities in experimental measurement and are surprisingly general: The proton spin cannot be explained by summing the intrinsic spins of its three constituent quarks (55). Inelastic scattering experiments reveal that the quark spins must be coupled to those of the gluons that hold them together (44).

Thermodynamic Cycles Measure Coupling Constants Between Perturbed Sites

A 2^N factorial experiment, the thermodynamic cycle (Figure 1), tests the impact on thermodynamic or kinetic behavior of all combinations of N perturbations. Point mutations report on discrete spatial regions, dissecting catalysis in space. Kinetics report on interactions along the reaction coordinate, dissecting in time. As in Φ-value analysis (77), free energy changes of coupled residues, $\Delta G^{\ddagger}$, are different for one mutant alone as opposed to the same mutation in the context of a second mutant. The discrepancy, $\Delta\Delta G^{\ddagger}$, measures the coupling free energy in kcal/mol, where the sign indicates whether coupling is synergistic (compensatory) or antisynergistic. Multiple mutations and other kinds of perturbations generalize the analysis; substituting Mn^{2+} for Mg^{2+} allows measurement of coupling to the metal.

Higher-Order Thermodynamic Cycles Are Necessary to Capture Three-Dimensional Behavior

Double-mutant cycles were introduced in biochemistry by Jencks (56, 58) and exploited by Fersht and colleagues (37, 39, 52) soon after directed mutagenesis made them feasible. A

double-mutant cycle has information about only a line, a triple mutant cycle about only a triangle. Neither is three-dimensional (103). Four-way perturbations are thus a minimum for capturing coordinated three-dimensional behavior implied by cooperative protein behavior. Higher-order cycles have not, however, been widely exploited, despite the fact that significant four- and five-way interactions with coupling energies (~4–6 kcal/mol) alter functionally important equilibria by up to 100,000-fold in examples reviewed herein (9, 35, 36, 38, 39, 96, 109, 111, 118). These coupling energies are quite distinct from the distributed behavior of multi-mutant cycles in other enzyme systems (100a) in which the intrinsic effects of individual side chains dominate.

MOLECULAR SWITCHES, MULTISTATE BEHAVIOR, AND HIGH-ORDER COUPLING

A molecular switch is a packing arrangement, within a monomer or between monomers in an oligomer, that assumes multiple configurations separated by a significant barrier. For example, hemoglobin alternates between relaxed (R) and tense (T) conformations in different crystal structures without populating intermediate states (79, 84). Alternative packing of β97 His occurs either between α38 Thr and α41 Thr in the R state or between α41 Thr and α44 Pro in the T state (8, figures 10a and 13). The resulting steric barrier precludes intermediate states.

Smith & Ackers (98) measured deviations in ligand-binding affinities from those expected from the affinities of monomers for the 10 different liganded forms of hemoglobin–indirectly from their dissociation into noncooperative α/β dimers. This cooperative free energy was 6 kcal/mol (98). Further, α/β dimers operate autonomously in the tetramer: Conversion of unliganded T state to high-affinity R state occurs if and only if both dimers have bound at least one ligand (51). Hemoglobin behaves as a three-level combinatorial switch responding to different ligand chemical potentials.

Identifying switching interactions in hemoglobin required an exhaustive catalog of differences between the R and T quaternary structures (8), a task unlikely to promote identifying switches in other multistate systems. However, the following examples illustrate that many conformational transitions proceed by rigid-body molecular motions, substantially reducing the number of dynamic packing interactions and facilitating automation of their identification.

Voltage-Gated K^+ Channel

The first determination of four-way residue coupling came from work on the voltage-gated K channel (9, 96, 118). Channel function is measured from a current versus voltage curve. Fitting to a Boltzmann sigmoid, assuming a two-state equilibrium between open and closed states (115), gives two parameters: the midpoint voltage, $V_{1/2}$, and the slope at the midpoint, Z. Scanning mutagenesis identified side chains whose mutation shifted this curve, changing the closed–open equilibrium. Residues with significant effects (Figure 2) were filtered by double-mutant cycles to detect long-range coupling (115).

Exhaustive double- and higher-order mutant cycles (96) clarified how the voltage-gated conformational change opens the pore to K^+ flux. The earlier study (115) discussed above identified four important properties: (*a*) mutations at many sites have little effect on the activation curve, highlighting mutationally sensitive positions above an insensitive background; (*b*) fitting parameters are correlated such that left-shifted activation curves exhibit steeper slopes; (*c*) residues in the activation gate are coupled to those in the selectivity filter; and (*d*) mutational perturbations of the activation curve parameters are linearly related to the free energy change of gating computed from a two-state model. The distance (up to 18 Å) between layers of coupled residues implied a large conformational change, as was observed (9, 96). Subsequent examination of higher-order coupling reinforced these preliminary conclusions in three ways (96).

A well-defined boundary exists between gating-sensitive and gating-insensitive sites—Yifrach & MacKinnon (115) defined the sensitive set as an allosteric trajectory. Average pairwise coupling free energies within the trajectory (Figure 2) were more than twice those measured between these residues and neighboring residues outside the trajectory. Coupling to a third residue is enhanced if the third residue is also within the trajectory (96). The high coupling energies are impressive because they occur between residues more than twice as far apart, on average, as the weakly coupled neighboring residues (48, 115). They demarcate the allosteric trajectory experimentally with remarkable precision.

Allosteric trajectories are highly cooperative—High synergy along the allosteric trajectory was confirmed by measuring four-way coupling free energies between the four residues comprising the trajectory, A391, E395, A465, and T469. In contrast to the a priori expectation that the higher-order interactions should decrease (12), mean *n*-way coupling energies increase approximately as n^2. The sign of $\Delta\Delta G_{\text{open}}$ for the four-way interaction implies that it contributes ~5 kcal/mol to the stability of the closed pore (96). Changes in membrane potential weaken these interactions, opening the pore.

The progressive increase in coupling energy is characteristic of cooperativity. The measured coupling free energy for a variant pore varies linearly with the steepness of the Boltzmann approximation to the voltage-activation curve. Yifrach (114) previously derived a relationship between that approximation and the Hill equation, in which the slopes of each curve have comparable meaning. As $\Delta\Delta G_{\text{open}} = -\Delta\Delta FZV_{1/2}$), where Z is the slope of the voltage-activation curve, Sadovsky & Yifrach (96) asked whether the nonlinearity of changes in the Hill coefficient arose from nonlinearity in Z or $V_{1/2}$. The large number of pore variants provided an unambiguous answer: $\Delta\Delta G_{\text{open}}$ is directly proportional to Z but unrelated to the midpoint voltage (96); the stronger the magnitude of high-order coupling, the more cooperative is the channel's gating transition.

General features of long-range coupling occur in other proteins—Observations relating results of combinatorial mutagenesis to experimental determinations of high-order coupling in staphylococcal nuclease (21, 22, 45) are of broader interest. Aliphatic side

chains within van der Waals contact behave differently, according to whether the perturbed residues belong to the allosteric trajectory. Neighboring residues outside the trajectory exhibit significantly reduced higher-order coupling than those within the trajectory (96). Trajectory-lining residues therefore exhibit a coupling behavior more similar to that observed between distant surface residues in staphylococcal nuclease (45), which interact via large coupling energies over large physical distances. Conversely, hydrophobic core interactions exhibit much reduced higher-order coupling. Similar conclusions emerged from related observations in the TrpRS system described below.

Tryptophanyl-tRNA Synthetase

TrpRS activates the tryptophan carboxylate with ATP, forming Trp-5′-adenylate plus pyrophosphate (PPi), a reaction that is the sine qua non for protein synthesis. TrpRS crystal structures have been solved without ligands (54) and complexed to substrates–-tryptophan, ATP (91); nonreactive substrate analog combinations–-tryptophanamide plus ATP (91); tryptophan plus AMP plus PPi (66); a transition-state analog—adenosine-5′-tetraphosphate (92); and products—Trp-5′-AMP (29, 93), Trp-5′-sulfoamyl-AMP, and Trp-methenyl-AMP (116). All structures fall into three clusters that are narrowly defined by two parameters: the hinge and twist angles between domains (62, 66). An open conformation is associated with the unliganded state; a closed, twisted conformation with the ATP-bound state; and a closed, untwisted conformation with the aminoacyl-AMP–bound state. The sequence of relative domain positions connects the three canonical stages—induced-fit, catalysis, and product release—of enzyme catalysis (16), and corresponds structurally and functionally to the three successive stages of ATP hydrolysis by the F1-ATPase β-subunit (1). Carter et al. previously suggested that three-state behavior might be necessary and sufficient for free energy transduction (16).

Allosteric coupling regulates catalytic assist by Mg^{2+}—Amino acid activation is assayed with the enzyme at equilibrium with both amino acid and ATP (24), so Michaelis–Menten parameters represent thermodynamic ground-state (K_M) and transition-state (k_{cat}) affinities. Native TrpRS accelerates tryptophan activation ~10^{14}-fold, apparently by stabilizing a dissociative transition state (16) in which the Mg^{2+} ion would help neutralize negative charge on the PPi leaving group. Mg^{2+} accelerates the reaction in water by at most fivefold (99). To determine how much Mg^{2+} accelerates the catalyzed rate, Carter & Weinreb rigorously eliminated metals from all solutions and added EDTA (ethylenediaminetetraacetic acid) to chelate the remaining metal ions. Mg^{2+} accelerates the TrpRS-catalyzed rate 100,000-fold (108), contributing −6.8 kcal/mol to transition-state stabilization, implying ~−6 kcal/mol of metal–enzyme coupling (Figure 3).

Identifying clusters of dynamic side chains—Many algorithms besides scanning mutagenesis have identified networks in proteins from correlated motions (13), phylogenetic conservation (71, 100), network analysis (11, 23, 26, 119), or NMR (nuclear magnetic resonance) relaxation (41). The functional significance of these networks must be validated, however, by higher-order thermodynamic cycle analysis. Kapustina identified switching regions computationally (Figure 4) using geometric and energetic filters (64) and molecular dynamics (62), reducing the number of possible mutants from 20^{328} to ~20; seven of these

sites compose the TrpRS D1 switch (18) (Figure 5*a*), a widely distributed (14) motif of conserved, neighboring residues that repack in crystal structures with different domain configurations (16, 54, 65, 91–93). These residues are connected to a larger cluster of dynamic surface residues.

High-order combinatorial variants implicate cooperative behavior of TrpRS D1 switch residues—In the high-energy pretransition state (64), Mg^{2+} competes with three lysine residues for one oxygen atom in each of the three phosphates, coupling it to the active site (Figure 6*a*). Molecular dynamics simulations (62, 63) showed that relaxing lysine–Mg^{2+} interactions allowed the domains to relax rapidly, either to the open or product conformations, thereby coupling them to the conformational state. That competition could thus account for the metal's catalytic assist. However, all possible mutations of these three lysines to alanine and glutamine showed that although the intrinsic effects of lysines and metal favored catalysis, their net coupling did not (112) (Figure 6*b*). The entire catalytic assist must arise from beyond the active site.

The D1 switch contains most of the residues that change packing partners during the shear created by induced-fit and catalytic domain motions. My laboratory (109) constructed all combinations of four of Rosetta's suggested mutations, I4V, F26L, Y33F, and F37I. Assaying all 16 variant proteins with Mg^{2+} and Mn^{2+} in triplicate afforded accurate estimation of all possible coupling energies and their uncertainties. By far the largest effect was the five-way coupling of all four residues to the metal (109) (Figure 7). The magnitude of this coupling energy, −5.0 kcal/mol, is approximately the amount by which Mg^{2+} stabilizes the transition state; the net D1 switch:Mg^{2} coupling accounts for −6.0 kcal/mol.

A modular variant cycle implicates domain movement in D1 switch residue coupling—A key innovation was to deconstruct TrpRS into functionally distinct modules derived from making aaRS Urzymes (15) —minimal invariant cores within the catalytic domain (68, 69, 86, 87) —by removing an insertion (connecting peptide 1, or CP1) and the anticodon-binding domain (ABD) (Figure 5*b*). The TrpRS Urzyme's activity allows it to serve as a molecular knockout anchoring a modular thermodynamic cycle involving the domains that move relative to one another during catalysis (Figure 8*a*). Each construct was catalytically active, leading to measurement of the intrinsic contributions to catalysis and specificity of CP1 and the ABD, and their energetic coupling (67). Neither catalysis nor specificity for tryptophan versus tyrosine benefitted from either module alone (Figure 8). Enhanced catalysis by Mg^{2+} (109) and specificity (111) arose only from their energetic coupling, ~−5 kcal/mol, in quantitative agreement with the five-way allosteric coupling described in the previous section. Given the quantitatively equivalent free energy coupling of D1 switch residues with Mg^{2+} and domain movement in the transition state, it is also reasonable that the domain motions are the simultaneous movements required for catalytic assist by Mg^{2+}.

PATH simulations: D1 switching is rate-limiting for domain movement—The computer program PATH (18, 20, 40) finds the sequence of structures that minimizes an action functional suggested by Onsager and Machlup (30, 81) that embeds a stochastic process in an overdamped, viscous medium governed by a Langevin equation. The algorithm

approximates the molecular physics as an elastic network. The resulting path is most probable because it has the least integrated difference between kinetic and potential energies, wasting the least energy. Energies are estimated for each structure; the highest energy structure is the conformational transition state.

PATH faithfully reproduces conformational transition-state structures found by other algorithms (7, 25), notably those produced by the string method (82). The transition-state structures it identifies are close to the stationary points of free energy surfaces (20) evaluated by discrete molecular dynamics (28, 97) on the two-dimensional conformational surface (66). TrpRS D1 switch residues F26, Y33, and F37 rearrange during the induced-fit transition. Unexpectedly similar aromatic side chain repacking imposes the barriers to two other, unrelated conformational changes (20). Thus, the D1 switch is not a unique switching mechanism.

The PATH program is fast enough for high-throughput studies. At convergence (20), PATH produces a four-tuple of approximate thermodynamic and kinetic parameters that influence catalysis: ΔG, the energy difference between initial and final conformations; t_{F_opt}, an asymptotic optimum total time; $U^{\ddagger}_{trans}$, the conformational barrier height; and $t_{\ddagger}$, the time to the transition state. PATH produces significantly different values for computational models of the 16 TrpRS structural D1 switch variants, facilitating quantitative comparison with experimental rates. Computational estimates correlate well with the experimental ΔG_{kcat} values for the same variants (19) (Figure 9), further tying experimental energetic coupling to conformational transition states.

CONCLUSIONS

Enzymes that couple free energy sources—electrostatic potentials, NTP hydrolysis, and so on—to work and/or information use sophisticated dynamic networks to transduce active-site chemistry into domain motions that change ligand and macromolecular binding affinities. To exhibit multistate behavior, a protein's conformation must have distinct potential energy wells, separated by saddle points with high conformational free energy. My laboratory and others have identified three-dimensional switching networks and used high-order combinatorial mutagenesis to map side chains responsible for equilibrium free energy differences (K channel) and rates of conformational changes (TrpRS) enabling transduction. TrpRS measurements were cross-validated by using modular cycles and identifying conformational transition-state structures computationally. The TrpRS conformational barrier closely resembles those in several unrelated systems. It is unclear whether a similar barrier keeps the voltage-gated K channel closed, because substate structures and allosteric coupling energies have yet to be determined for the same protein. Several themes nevertheless unify the two systems.

K Channel Coupling Energies Are Anisotropic and Highly Cooperative

Although the combinatorial thermodynamic cycles for the two model systems discussed here are equivalent in principle, their uses differ. Yifrach (9, 96, 115) carefully compared coupling energetics for on- and off-trajectory interactions, revealing what he calls the

"anisotropic boundaries" of the allosteric trajectory. This conclusion justifies, post hoc, the assumption that dynamic coupling within rigid bodies can be ignored, as Kapustina (64) did with TrpRS. High-order coupling free energies and cooperativity are also more carefully connected for the K pore opening. However, as the readout is thermodynamic rather than kinetic, the link between cooperativity and coordinated motion is less secure than in the TrpRS studies (18, 19, 64, 67, 108–111), in which the readout, $\Delta G^{\ddagger}$, necessarily implies coordinated motion of all four side chains from the D1 molecular switch with the active-site Mg^{2+} in the transient state for amino acid activation, and in which the most probable path ensemble has been characterized.

TrpRS Multistate Behavior Is Coupled to Catalysis and Hence Implies Motion

TrpRS coupling energies for k_{cat} represent interactions that form only transiently in the transition state. Hence, TrpRS modules must move relative to one another to generate them, as noted above for directed mutagenesis of the TyrRS active site (32–34, 39). Combinatorial point and modular thermodynamic cycles give similar energetics. Both catalysis and specificity in full-length TrpRS are therefore coupled by ~5 kcal/mol to the switching region where domain movement generates shear and to the simultaneous motion of the two domains relative to the Urzyme.

Single-turnover experiments indicate that the intrinsic chemical step proceeds in milliseconds, consistent with domain motion, and is strongly correlated with the pattern of point mutations in the switching region remote from the active site (Figure 9), validating the conclusion that the 10^5-fold catalytic acceleration by Mg^{2+} requires domain motion. Energetic coupling thus reinforces earlier suggestions (16, 91, 92, 117) that differences observed between TrpRS crystal structures are relevant to the catalytic cycle. Simultaneous motions of CP1 and the ABD are necessary for fully functional TrpRS catalysis and specific tryptophan recognition: In the absence of either domain, the overall rate acceleration falls by ~10^{-5}-fold and the free energy of discriminating between tryptophan and tyrosine falls from ~6 kcal/mol to 1 kcal/mol (67), which is almost exactly as the Urzyme alone behaves.

Domain Motions Cannot Contribute Directly to Transition-State Stabilization

Warshel & Bora (106) note that domain motions are far too slow, leading to dissipation of their kinetic energies, and the molecular forces generated too weak to couple directly to catalysis. Thus, domain movement itself cannot actually lower the transition-state energy. Rather, TrpRS domain motion appears to contribute to transient active-site preorganization (88), actually slowing the chemistry relative to that possible in a static active site. Deceleration thus ensures coupling of catalysis to conformational change. This hypothesis accounts for two observations that previously seemed unrelated: (*a*) single-turnover rates show that the chemical step occurs in milliseconds, that is, the time frame of domain motions, and (*b*) the rate of the chemical step, k_{chem}, is closely correlated ($P_F < 0.0001$) to the D1 switch mutations and their higher-order interactions (Figure 9). Structural perturbations thus influence only the chemical step of the reaction. Turnover is uncorrelated, reinforcing the conclusion that the catalytic step is coupled to domain motion.

TrpRS domain motions appear to constitute a timing mechanism for active-site preorganization. Each TrpRS conformation has distinctive ligand affinities (66, 91, 92), including configurations associated with the transition state. Catalysis cannot occur unless the domains change orientation (109). Preorganization of the catalytic metal ion is thus orchestrated to couple differential affinity changes associated with ATP binding, hydrolysis, and product release to the domain configuration, ensuring that ATP hydrolysis occurs if and only if the conformation changes (110).

The TrpRS catalytic domain movement becomes thermodynamically favorable only after PPi release (20). This behavior resembles that observed for myosin, as its power stroke is initiated by orthophosphate release, whereas release of ADP happens only as the power stroke proceeds toward the rigor state (73–75). Orthophosphate and PPi are much more strongly solvated than is ATP (113). Using differential solvation free energies to shift conformational equilibria appears to be another important mechanism ensuring that catalysis is coupled to (subsequent) domain movement. Early release of phosphoryl/pyrophosphoryl groups may exemplify even more widely used mechanisms contributing to vectorial domain motion in transducing enzymes.

Conformational Coupling, Vectorial Behavior, and Free Energy Transduction

Jencks (60, 61) outlined how sequential changes in ligand affinity lead to changes in the overall free energy of ATP hydrolysis within an active site, and recognized the need for coupling rules. However, as structural landscapes were then unknown, Jencks was mute about what mechanisms actually linked conformational changes to catalysis. Identifying (62, 64) and mutating (110, 112) key molecular switching residues and modular thermodynamic cycles (67) that measure energetic coupling between domains have now clarified how idiosyncratic structural and mechanistic details implement coupling rules.

Molecular machines work by stochastic diffusive processes—In contrast to macrolevel machines, directionality in molecular machines arises from processes that, by microscopic reversibility, operate at mechanical equilibrium and require coupling domain movements to an energy source (3–6). Motor proteins must therefore couple conformational equilibria fully to catalyzed NTP hydrolysis.

Three states enable ratcheting: the verge and Foliot clockwork—Astumian (5) uses an ingenious synthetic molecular motor (47) mimicking a peristaltic pump to illustrate that two catenated rings are sufficient to capture coupled vectorial behavior in the net rotation of both rings (57) coupled either to pH- or redox-induced changes in a catenated organic ring system, implementing a ratchet. Because one catenane blocks the reverse motion of the other, a ratchet of this sort requires three states. The escapement in a mechanical clockwork (95; 109, figure 5) furnishes another metaphor. Transducing molecular machines have at least three distinct conformational ensembles (1, 16), corresponding to the unliganded, the triphosphate, and the diphosphate complexes. Coupling catalysis of NTP hydrolysis to domain motion and exergonic ligand dissociation appear to be complementary sources of directionality.

Toward Long-Range Global Coupling Maps for Proteins

The consistency of allosteric coupling energies in three unrelated systems—6 kcal/mol for hemoglobin, 5 kcal/mol for the K^+ channel, and 5 kcal/mol for combinatorial and modular coupling for TrpRS—suggests that long-range coupling may saturate such that interactions of order >4 rarely, if ever, exceed such values. Work reviewed here is thus only a snapshot of an unexplored but important and accessible landscape. Both Sadovsky & Yifrach (96) and Kapustina and colleagues (64) simplify global site–site coupling distributions into binary sets with strong versus weak coupling, as suggested by Greed & Shortle (45). As such distributions enhance understanding of biological function, it is probably worth reexamining Greed & Shortle's (45) and Chen & Stites's (21, 22) coupling data for staphylococcal nuclease and correlating its approximate, global coupling map to its enzymatic function.

Each TrpRS switching region connects with a cluster of dynamic surface residues (64). It is puzzling that the conservative D1 switch mutations suggested by Rosetta should have only minimal impact on the relative stability of different state conformations (64). How then do those perturbations give rise to coupling energies of −5 kcal/mol? SNAPP (Simplicial Neighbor Analysis of Protein Packing) analysis (17, 64) suggests that these peri-core networks may use the strength of differential interactions with water to amplify the energetic impact of core repacking. High-dimensional analysis of coupling between core and peri-core residues could address this question.

Acknowledgments

Special thanks are due to A. Lee for emphasizing nonadditivity and identifying work of O. Yifrach. H. Fried (Cursor Scientific Editing and Writing, LLC) and R.D. Astumian made many helpful suggestions on the manuscript. Research at the University of North Carolina was supported by the National Institute of General Medical Sciences (NIGMS 90406 and 78227).

LITERATURE CITED

1. Abrahams JP, Leslie AGW, Lutter R, Walker JE. Structure at 2.8 Å resolution of F_1-ATPase from bovine heart mitochondria. Nature. 1994; 370:621–28. [PubMed: 8065448]
2. Adamczyk AJ, Warshel A. Converting structural information into an allosteric-energy-based picture for elongation factor Tu activation by the ribosome. PNAS. 2011; 108:9827–32. [PubMed: 21617092]
3. Astumian RD. Design principles for Brownian molecular machines: how to swim in molasses and walk in a hurricane. Phys Chem Chem Phys. 2007; 9:5067–83. [PubMed: 17878982]
4. Astumian RD. Thermodynamics and kinetics of molecular motors. Biophys J. 2010; 98:2401–9. [PubMed: 20513383]
5. Astumian RD. Stochastic conformational pumping: a mechanism for free-energy transduction by molecules. Annu Rev Biophys. 2011; 40:289–313. [PubMed: 21351880]
6. Astumian RD, Mukherjee S, Warshel A. The physics and physical chemistry of molecular machines. Chem Phys Chem. 2016; 17:1719–41. [PubMed: 27149926]
7. Bahar I, Lezon TR, Yang L-W, Eyal E. Global dynamics of proteins: bridging between structure and function. Annu Rev Biophys. 2010; 39:23–42. [PubMed: 20192781]
8. Baldwin J, Chothia C. Hemoglobin: the structural changes related to ligand binding and its allosteric mechanism. J Mol Biol. 1979; 129:175–200. [PubMed: 39173]
9. Ben-Abu Y, Zhou Y, Zilberberg N, Yifrach O. Inverse coupling in leak and voltage-activated K^+ channel gates underlies distinct roles in electrical signaling. Nat Struct Mol Biol. 2009; 16:71–79. [PubMed: 19098918]

10. Deleted in proof
11. Berezhkovskii A, Hummer G, Szabo A. Reactive flux and folding pathways in network models of coarse-grained protein dynamics. J Chem Phys. 2009; 130:205102. [PubMed: 19485483]
12. Box, GEP., Hunter, WG., Hunter, JS. Statistics for Experimenters. New York: Wiley Interscience; 1978.
13. Budiman M, Knaggs MH, Fetrow JS, Alexander RW. Using molecular dynamics to map interaction networks in an aminoacyl-tRNA synthetase. Proteins. 2007; 68:670–89. [PubMed: 17510965]
14. Cammer S, Carter CW Jr. Six Rossmannoid folds, including the Class I aminoacyl-tRNA synthetases, share a partial core with the anticodon-binding domain of a Class II aminoacyl-tRNA synthetase. Bioinformatics. 2010; 26:709–14. [PubMed: 20130031]
15. Carter CW Jr. Urzymology: experimental access to a key transition in the appearance of enzymes. J Biol Chem. 2014; 289:30213–20. [PubMed: 25210034]
16. Carter, CW., Jr, Ilyin, V., Yin, Y., Huang, X., Retailleau, P. Three TrpRS conformations stabilize a dynamic, dissociative transition-state; Presented at Using Crystallogr. Underst. Enzym. Mech.; St. Paul, MN. 2001.
17. Carter CW Jr, LeFebvre B, Cammer SA, Tropsha A, Edgell MH. Four-body potentials reveal protein-specific correlations to stability changes caused by hydrophobic core mutations. J Mol Biol. 2001; 311:625–38. [PubMed: 11518520]
18. Carter J, Charles W, Chandrasekaran SN, Weinreb V, Li L, Williams T. Combining multi-mutant and modular thermodynamic cycles to measure energetic coupling networks in enzyme catalysis. Struct Dyn. 2017 In press.
19. Chandrasekaran SN, Carter CWJ. Adding torsional interaction terms to the Anisotropic Network Model improves the PATH performance, enabling detailed comparison with experimental rate data. Struct Dyn. 2017 In press.
20. Chandrasekaran SN, Das J, Dokholyan V, Carter JCW. A modified PATH algorithm rapidly generates transition states comparable to those found by other well established algorithms. Struct Dyn. 2016; 3:012101. [PubMed: 26958584]
21. Chen J, Stites WE. Energetics of side chain packing in staphylococcal nuclease assessed by systematic double mutant cycles. Biochemistry. 2001; 40:14004–11. [PubMed: 11705392]
22. Chen J, Stites WE. Higher-order packing interactions in triple and quadruple mutants of staphylococcal nuclease. Biochemistry. 2001; 40:14012–19. [PubMed: 11705393]
23. Chi C, Elfström L, Shi Y, Snäll T, Engström A, Jemth P. Reassessing a sparse energetic network within a single protein domain. PNAS. 2008; 105:4679–84. [PubMed: 18339805]
24. Cleland WW, Northrup DB. Energetics of substrate binding, catalysis, and product release. Methods Enzymol. 1999; 308:3–48. [PubMed: 10506998]
25. Das A, Gur M, Cheng MH, Jo S, Bahar I, Roux B. Exploring the conformational transitions of biomolecular systems using a simple two-state anisotropic network model. PLOS Comput Biol. 2014; 10:e1003521. [PubMed: 24699246]
26. del Sol A, Fujihashi H, Amoros D, Nussinov R. Residues crucial for maintaining short paths in network communication mediate signaling in proteins. Mol Syst Biol. 2006; 2(2006):0019. [PubMed: 16738564]
27. Dill, KA., Bromberg, S. Molecular Driving Forces. New York: Garland; 2012.
28. Dokholyan V, Buldyrev SV, Stanley HE, Shakhnovich EI. Discrete molecular dynamics studies of the folding of a protein-like model. Fold Des. 1998; 3:577–87. [PubMed: 9889167]
29. Doublié S, Bricogne G, Gilmore CJ, Carter CW Jr. Tryptophanyl-tRNA synthetase crystal structure reveals an unexpected homology to tyrosyl-tRNA synthetase. Structure. 1995; 3:17–31. [PubMed: 7743129]
30. Dürr D, Bach A. The Onsager-Machlup function as a Lagrangian for the most probable path of a diffusion process. Commun Math Phys. 1978; 60:153–70.
31. Eisenberg E, Hill TL. A cross-bridge model of muscle contraction. Prog Biophys Mol Biol. 1978; 33:55–82. [PubMed: 146885]

32. Fersht AR. Dissection of the structure and activity of the tyrosyl-tRNA synthetase by site-directed mutagenesis. Biochemistry. 1987; 26:8031–37. [PubMed: 3442641]
33. Fersht AR, Knill Jones JW, Bedouelle H, Winter G. Reconstruction by site-directed mutagenesis of the transition state for the activation of tyrosine by the tyrosyl-tRNA synthetase: A mobile loop envelopes the transition state in an induced-fit mechanism. Biochemistry. 1988; 27:1581–87. [PubMed: 3284584]
34. First EA, Fersht AR. Involvement of threonine 234 in catalysis of tyrosyl adenylate formation by tyrosyl-tRNA synthetase. Biochemistry. 1993; 32:13644–50. [PubMed: 8257697]
35. Deleted in proof
36. First EA, Fersht AR. Mutation of lysine 233 to alanine introduces positive cooperativity into tyrosyl-tRNA synthetase. Biochemistry. 1993; 32:13651–57. [PubMed: 8257698]
37. First EA, Fersht AR. Mutational and kinetic analysis of a mobile loop in tyrosyl-tRNA synthetase. Biochemistry. 1993; 32:13658–63. [PubMed: 8257699]
38. Deleted in proof
39. First EA, Fersht AR. Analysis of the role of the KMSKS loop in the catalytic mechanism of the tyrosyl-tRNA synthetase using multimutant cycles. Biochemistry. 1995; 34:5030–43. [PubMed: 7711024]
40. Franklin J, Koehl P, Doniach S, Delarue M. MinActionPath: maximum likelihood trajectory for large-scale structural transitions in a coarse-grained locally harmonic energy landscape. Nucleic Acids Res. 2007; 35:W477–82. [PubMed: 17545201]
41. Fuentes EJ, Gilmore SA, Mauldin RV, Lee AL. Evaluation of energetic and dynamic coupling networks in a PDZ domain protein. J Mol Biol. 2006; 364:337–51. [PubMed: 17011581]
42. Gao R, Mack TR, Stock AM. Bacterial response regulators: versatile regulatory strategies from common domains. TRENDS Biochem Sci. 32:225–34.
43. Ge H, Pressé S, Ghosh K, Dill KA. Markov processes follow from the principle of maximum caliber. J Chem Phys. 2012; 136:064108. [PubMed: 22360170]
44. Goldenfield, N. Individuality. In: Brockman, J., editor. This Idea Must Die: Scientific Theories That Are Blocking Progress. New York: Harper Perennial; 2015. p. 25-28.
45. Greed SM, Shortle D. Patterns of nonadditivity between pairs of stability mutations in staphylococcal nuclease? Biochemistry. 1993; 32:10131–39. [PubMed: 8399139]
46. Gunasekaran K, Buyong M, Nussinov R. Is allostery an intrinsic property of all dynamic proteins? Proteins. 2004; 57:433–43. [PubMed: 15382234]
47. Hernandez JV, Kay ER, Leigh DA. A reversible synthetic rotary molecular motor. Science. 2004; 306:1532–37. [PubMed: 15567858]
48. Hidalgo P, MacKinnon R. Revealing the architecture of a K^+ channel pore through mutant cycles with a peptide inhibitor. Science. 1995; 268:307–10. [PubMed: 7716527]
49. Hill TL. Some general principles in free energy transduction. PNAS. 1983; 80:2922–25. [PubMed: 6222376]
50. Hill TL, Eisenberg E. Can free energy transduction be localized at some crucial part of the enzymatic cycle? Q Rev Biophys. 1981; 14:463–511. [PubMed: 7034036]
51. Holt JM, Ackers GK. The pathway of allosteric control as revealed by hemoglobin intermeditate states. FASEB J. 1995; 9:210–18. [PubMed: 7781923]
52. Horovitz A, Fersht AR. Strategy for analyzing the cooperativity of intramolecular interactions in peptides and proteins. J Mol Biol. 1990; 214:613–17. [PubMed: 2388258]
53. Howard, J. Mechanics of Motor Proteins and the Cytoskeleton. Sunderland, MA: Sinauer; 2001.
54. Ilyin VA, Temple B, Hu M, Li G, Yin Y, et al. 2.9 Å Crystal structure of ligand-free tryptophanyl-tRNA synthetase: Domain movements fragment the adenine nucleotide binding site. Protein Sci. 2000; 9:218–31. [PubMed: 10716174]
55. Jaffe R. Where does the proton really get its spin? Phys Today. 1995; 48:24–30.
56. Jencks WP. Binding energy, specificity, and enzymatic catalysis: the Circe effect. Adv Enzymol Relat Areas Mol Biol. 1975; 43:219–410. [PubMed: 892]
57. Jencks WP. The utilization of binding energy in coupled vectorial processes. Adv Enzymol Relat Areas Mol Biol. 1980; 51:75–106. [PubMed: 6255774]

58. Jencks WP. On the attribution and additivity of binding energies. PNAS. 1981; 78:4046–50. [PubMed: 16593049]
59. Jencks, WP. Catalysis in Chemistry and Enzymology. New York: Dover; 1987.
60. Jencks WP. Utilization of binding energy and coupling rules for active transport and other coupled vectorial processes. Methods Enymol. 1989; 171:145–64.
61. Jencks WP. Reaction mechanisms, catalysis, and movement. Protein Sci. 1994; 3:2459–64. [PubMed: 7757002]
62. Kapustina M, Carter CW Jr. Computational studies of tryptophanyl-tRNA synthetase ligand binding and conformational stability. J Mol Biol. 2006; 362:1159–80. [PubMed: 16949606]
63. Kapustina M, Hermans J, Carter CW Jr. Potential of mean force estimation of the relative magnitude of the effect of errors in molecular mechanics approximations. J Mol Biol. 2006; 362:1177–80.
64. Kapustina M, Weinreb V, Li L, Kuhlman B, Carter CW Jr. A conformational transition state accompanies tryptophan activation by *B. stearothermphilus* tryptophanyl-tRNA synthetase. Structure. 2007; 15:1272–84. [PubMed: 17937916]
65. Laowanapiban P, Kapustina M, Vonrhein C, Delarue M, Koehl P, Carter CW Jr. Independent saturation of three TrpRS subsites generates a partially-assembled state similar to those observed in molecular simulations. PNAS. 2009; 106:1790–95. [PubMed: 19174517]
66. Laowanapiban P, Kapustina M, Vonrhein C, Delarue M, Koehl P, Carter CW Jr. Independent saturation of three TrpRS subsites generates a partially-assembled state similar to those observed in molecular simulations. PNAS. 2009; 106:1790–95. [PubMed: 19174517]
67. Li L, Carter CW Jr. Full implementation of the genetic code by tryptophanyl-tRNA synthetase requires intermodular coupling. J Biol Chem. 2013; 288:34736–45. [PubMed: 24142809]
68. Li L, Francklyn C, Carter CW Jr. Aminoacylating Urzymes challenge the RNA World hypothesis. J Biol Chem. 2013; 288:26856–63. [PubMed: 23867455]
69. Li L, Weinreb V, Francklyn C, Carter CW Jr. Histidyl-tRNA synthetase Urzymes: Class I and II aminoacyl-tRNA synthetase Urzymes have comparable catalytic activities for cognate amino acid activation. J Biol Chem. 2011; 286:10387–95. [PubMed: 21270472]
70. Liao J-C, Sun S, Chandler D, Oster G. The conformational states of Mg•ATP in water. Eur Biophys J. 2004; 33:29–37. [PubMed: 12904910]
71. Lockless SW, Ranganathan R. Evolutionarily conserved pathways of energetic connectivity in protein families. Science. 1999; 286:295–99. [PubMed: 10514373]
72. Long SB, Campbell EB, MacKinnon R. Crystal structure of a mammalian voltage-dependent *Shaker* family K^+ channel. Science. 2005; 309:897–903. [PubMed: 16002581]
73. Lymn RW. Kinetic analysi of myosin and actomyosin ATPase. Annu Rev Biophys Bioeng. 1979; 8:145–63. [PubMed: 157716]
74. Lymn RW, Taylor EW. Transient state phosphate production in the hydrolysis of nucleoside triphospahes by myosin. Biochemistry. 1970; 9:2975–83. [PubMed: 4248809]
75. Lymn RW, Taylor EW. Mechanism of adenosine triphosphate hydrolysis by actomyosin. Biochemistry. 1971; 10:4617–24. [PubMed: 4258719]
76. Martinez L, Jimenez-Rodriguez M, Gonzalez-Rivera K, Williams T, Li L, et al. Functional Class I and II amino acid activating enzymes can be coded by opposite strands of the same gene. J Biol Chem. 2015; 290:19710–25. [PubMed: 26088142]
77. Matouschek A, Fersht AR. Protein engineering in analysis of protein folding pathways and stability. Methods Enzymol. 1991; 202:82–112. [PubMed: 1784198]
78. Monod J, Changeux J-P, Jacob F. Allosteric proteins and cellular control systems. J Mol Biol. 1963; 6:306–29. [PubMed: 13936070]
79. Monod J, Wyman J, Changeux J-P. On the nature of allosteric transitions: a plausible model. J Mol Biol. 1965; 12:88–118. [PubMed: 14343300]
80. Motlagh HN, Wrabl JO, Li J, Hilser VJ. The ensemble nature of allostery. Nature. 2014; 508:331–39. [PubMed: 24740064]
81. Onsager L, Machlup S. Fluctuations and irreversible processes. Phys Rev. 1953; 91:1505–12.

82. Ovchinnikov V, Karplus M, Vanden-Eijnden E. Free energy of conformational transition paths in biomolecules: the string method and its application to myosin VI. J Chem Phys. 2011; 134:085103. [PubMed: 21361558]

83. Ovchinnikov V, Trouta BL, Karplus M. Mechanical coupling in myosin V: a simulation study. J Mol Biol. 2010; 395:815–35. [PubMed: 19853615]

84. Perutz MF. Stereochemistry of cooperative effects of hemoglobin. Nature. 1970; 228:726–39. [PubMed: 5528785]

85. Petit CM, Zhang J, Fuentes EJ, Lee AL. Hidden dynamic allostery in a PDZ domain. PNAS. 2009; 46:18249–54.

86. Pham Y, Kuhlman B, Butterfoss GL, Hu H, Weinreb V, Carter CW Jr. Tryptophanyl-tRNA synthetase Urzyme: a model to recapitulate molecular evolution and investigate intramolecular complementation. J Biol Chem. 2010; 285:38590–601. [PubMed: 20864539]

87. Pham Y, Li L, Kim A, Weinreb V, Butterfoss G, et al. A minimal TrpRS catalytic domain supports sense/antisense ancestry of Class I and II aminoacyl-tRNA synthetases. Mol Cell. 2007; 25:851–62. [PubMed: 17386262]

88. Prasad BR, Warshel A. Prechemistry versus preorganization in DNA replication fidelity. Proteins. 2011; 79:2900–19. [PubMed: 21905114]

89. Pressé S, Ghosh K, Dill KA. Modeling stochastic dynamics in biochemical systems with feedback using maximum caliber. J Phys Chem. 2011; B115:6202–12.

90. Rees DC, Howard JB. Structural bioenergetics and energy transduction mechanisms. J Mol Biol. 1999; 293:343–50. [PubMed: 10550213]

91. Retailleau P, Huang X, Yin Y, Hu M, Weinreb V, et al. Interconversion of ATP binding and conformational free energies by tryptophanyl-tRNA synthetase: structures of ATP bound to open and closed, pre-transition conformations. J Mol Biol. 2003; 325:39–63. [PubMed: 12473451]

92. Retailleau P, Weinreb V, Hu M, Carter CW Jr. Crystal structure of tryptophanyl-tRNA synthetase complexed with adenosine-5′ tetraphosphate: evidence for distributed use of catalytic binding energy in amino acid activation by Class I aminoacyl-tRNA synthetases. J Mol Biol. 2007; 369:108–28. [PubMed: 17428498]

93. Retailleau P, Yin Y, Hu M, Roach JM, Bricogne G, et al. High resolution experimental phases for tryptophanyl-tRNA synthetase (TrpRS) complexed with tryptophanyl-5′AMP. Acta Crystallogr D. 2001; 57:1595–608. [PubMed: 11679724]

94. Rosenfeld SS, Houdusse A, Sweeney HL. Magnesium regulates ADP dissociation from myosin V. J Biol Chem. 2005; 280:6072–79. [PubMed: 15579901]

95. Roup AV, Bernstein DS, Neresov SG, Hadda WM, Chellaboina V. Limit cycle analysis of the verge and Foliot clock escapement using impulsive differential equations and Poincaré maps. Int J Control. 2003; 76:1685–98.

96. Sadovsky E, Yifrach O. Principles underlying energetic coupling along an allosteric communication trajectory of a voltage-activated K channel. PNAS. 2007; 104:19813–18. [PubMed: 18077413]

97. Shirvanyants D, Ding F, Tsao D, Ramachandran S, Dokholyan V. Discrete molecular dynamics: an efficient and versatile simulation method for fine protein characterization. J Phys Chem B. 2012; 116:8375–82. [PubMed: 22280505]

98. Smith FR, Ackers GK. Experimental resolution of cooperative free energies for the ten ligation states of human hemoglobin. PNAS. 1985; 82:5347–51. [PubMed: 3860865]

99. Stockbridge RB, Wolfenden R. The intrinsic reactivity of ATP and the catalytic proficiencies of kinases acting on glucose, N-acetylglucosamine, and homoserine. J Biol Chem. 2009; 284:22747–57. [PubMed: 19531469]

100. Suel GM, Lockless SW, Wall MA, Ranganathan R. Evolutionarily conserved networks of residues mediate allosteric communication in proteins. Nat Struct Biol. 2003; 10:59–69. [PubMed: 12483203]

100a. Sunden F, Peck A, Salzman J, Ressl S, Herschlag D. Extensive site-directed mutagenesis reveals interconnected functional units in the alkaline phosphatase active site. eLife. 2015; 4:e06181.

101. Sweeney HL, Houdusse A. Myosin VI rewrites the rules for myosin motors. Cell. 2010; 141:573–82. [PubMed: 20478251]

102. Sweeney HL, Houdusse A. Structural and functional insights into the myosin motor mechanism. Annu Rev Biophys. 2010; 39:539–57. [PubMed: 20192767]
103. Thomas PD, Dill KA. Statistical potentials extracted from protein structures: How accurate are they? J Mol Biol. 1996; 257:457–69. [PubMed: 8609636]
104. Tsai C-J, Nussinov R. A unified view of "how allostery works. PLOS Comput Biol. 2014; 10:e1003394. [PubMed: 24516370]
105. Vanden-Eijndena E, Venturolib M. Revisiting the finite temperature string method for the calculation of reaction tubes and free energies. J Chem Phys. 2009; 130:194103. [PubMed: 19466817]
106. Warshel A, Bora RP. Perspective: defining and quantifying the role of dynamics in enzyme catalysis. J Chem Phys. 2016; 144:180901. [PubMed: 27179464]
107. Weinkam P, Ponsb J, Sali A. Structure-based model of allostery predicts coupling between distant sites. PNAS. 2012; 109:4875–80. [PubMed: 22403063]
108. Weinreb V, Carter CW Jr. Mg^{2+}-free *B. stearothermophilus* tryptophanyl-tRNA synthetase activates tryptophan with a major fraction of the overall rate enhancement. J Am Chem Soc. 2008; 130:1488–94. [PubMed: 18173270]
109. Weinreb V, Li L, Carter CW Jr. A master switch couples Mg^{2+}-assisted catalysis to domain motion in *B. stearothermophilus* tryptophanyl-tRNA synthetase. Structure. 2012; 20:128–38. [PubMed: 22244762]
110. Deleted in proof
111. Weinreb V, Li L, Chandrasekaran SN, Koehl P, Delarue M, Carter CW Jr. Enhanced amino acid selection in fully-evolved tryptophanyl-tRNA synthetase, relative to its Urzyme, requires domain movement sensed by the D1 Switch, a remote, dynamic packing motif. J Biol Chem. 2014; 289:4367–76. [PubMed: 24394410]
112. Weinreb V, Li L, Kaguni LS, Campbell CL, Carter CW Jr. Mg2+-assisted catalysis by *B. stearothermophilus* TrpRS is promoted by allosteric effects. Structure. 2009; 17:1–13. [PubMed: 19141274]
113. Wolfenden R, Williams R. Affinities of phosphoric acids, esters and amides for solvent water. J Am Chem Soc. 1983; 105:1028–31.
114. Yifrach O. Hill coefficient for estimating the magnitude of cooperativity in gating transitions of voltage-dependent ion channels. Biophys J. 2004; 87:822–30. [PubMed: 15298891]
115. Yifrach O, MacKinnon R. Energetics of pore opening in a voltage-gated K channel. Cell. 2002; 111:231–39. [PubMed: 12408867]
116. Yin, Y. PhD Thesis. Univ. N.C.; Chapel Hill: 1995. *Crystallographic study of* Bacillus stearothermophilus *tryptophanyl-tRNA synthetase in the catalytic reaction*.
117. Yin Y, Carter CW Jr. Quantitative analysis in the characterization and optimization of protein crystal growth. Acta Crystallogr D. 1994; 50:572–90. [PubMed: 15299421]
118. Zandany N, Ovadia M, Orr I, Yifrach O. Direct analysis of cooperativity in multisubunit allosteric proteins. PNAS. 2008; 105:11697–702. [PubMed: 18687896]
119. Zheng W, Brooks BR, Doniach S, Thirumalai D. Network of dynamically important residues in the open/closed transition in polymerases is strongly conserved. Structure. 2005; 13:565–77. [PubMed: 15837195]

SUMMARY POINTS

1. High-dimensional thermodynamic cycles are necessary to capture three-dimensional allosteric effects.
2. Rigid-body domain motion simplifies identification of molecular switches from the intersection of dynamic Delaunay tetrahedra and energetically sensitive sites.
3. TrpRS transition state stabilization increases by ~6 kcal/mol if and only if the domains move, changing the configuration of the rate-limiting D1 switch and preorganizing the active site.
4. TrpRS side chains that move coordinately with catalysis to ensure catalytic assist by Mg^{2+} are broadly conserved and remote from the active site.
5. A modular thermodynamic cycle confirmed that the same coupling energy promotes both catalysis and specificity in full-length TrpRS.
6. PATH parameters correlate with experimental single-turnover rates of combinatorial point mutants.
7. Multiple aromatic group repacking creates conformational transition states in three unrelated systems.
8. Making ATP hydrolysis conditional to domain motion optimizes efficiency of molecular motors.

FUTURE ISSUES

1. TrpRS coupling is ambiguous; inter- and intrasubunit coupling in the homodimer can be distinguished by measuring coupling in heterodimeric TrpRSs, as noted herein (118).
2. Higher-order cycles can confirm coupling between remote sites and active-site residues.
3. It is important to determine whether or not coupling energies saturate.
4. Differential surface interactions may well exploit the role of water to amplify energy differences triggered by core residue switching. It is worth examining how this relates to the proposals of Greed and Shortle (45).

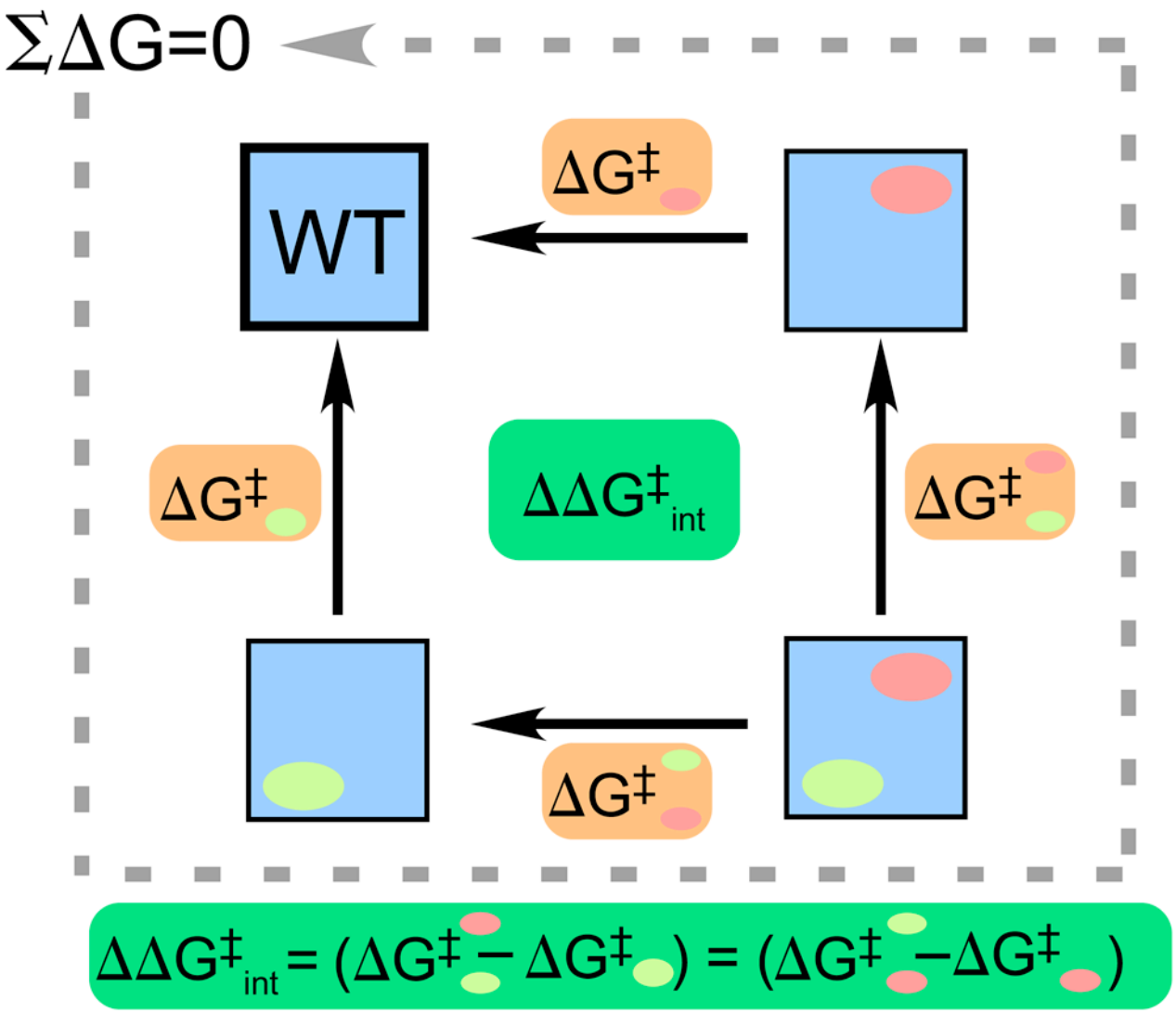

Figure 1.
A double-mutant thermodynamic cycle (18). Factorial design measures the impact of mutation at one site (*green*) in the context of mutation at a second site (*salmon*). As the total free energy change is zero for the circuit, nonadditivities of opposite edges are equal and estimate coupling energies between perturbed sites. Abbreviation: WT, wild type. Figure adapted from Reference 20 with permission from AIP Publishing.

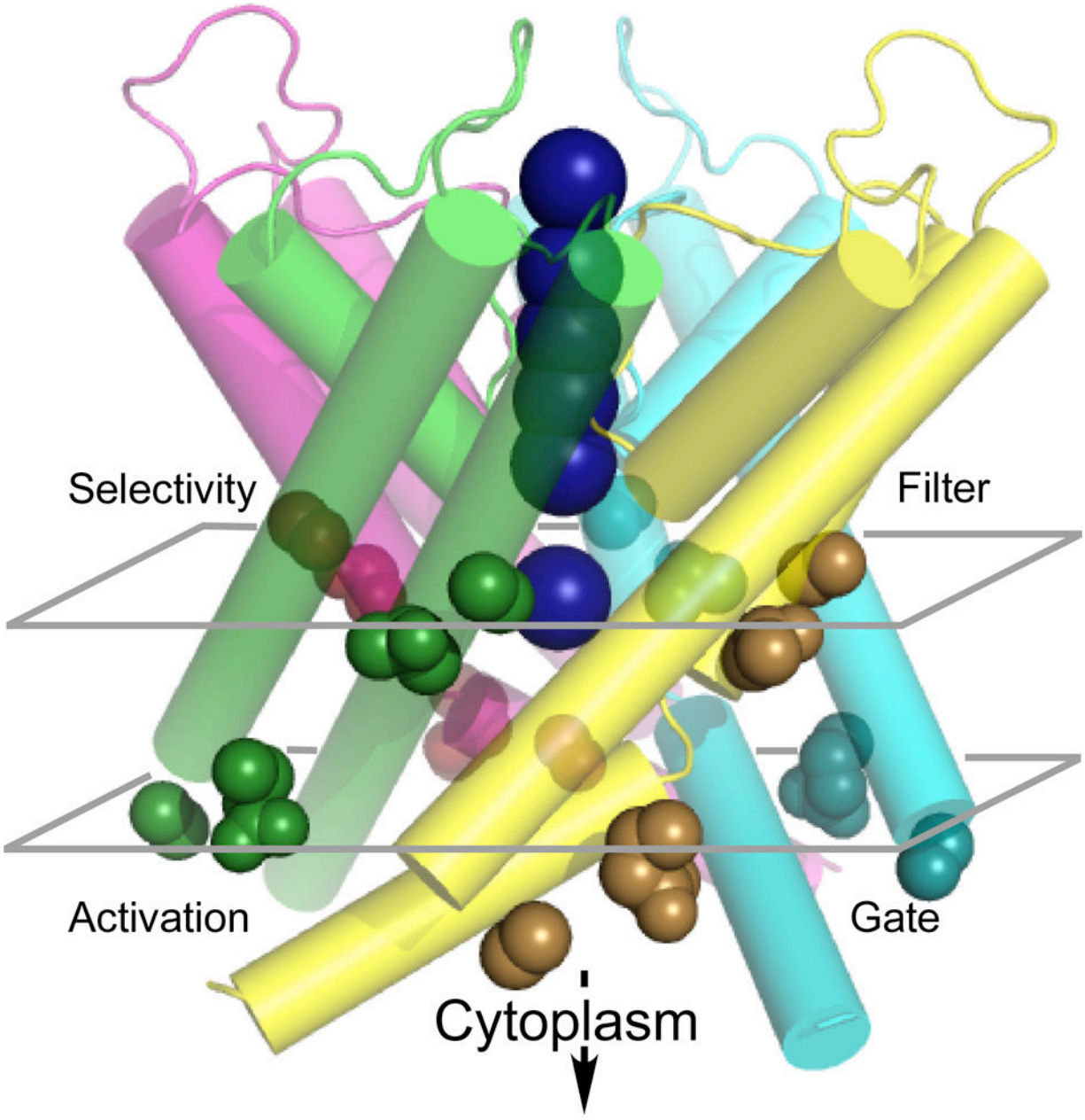

Figure 2.

The Shaker Kv channel (72) pore domain (PDB 2A79). C-terminal residues of four monomers that form the tetrameric pore are represented in different colors. Spheres are side chains identified to have large two-way coupling energies; they occur in the activation gate and selectivity filter. Potassium ions from crystal structures are also shown (*dark blue spheres*).

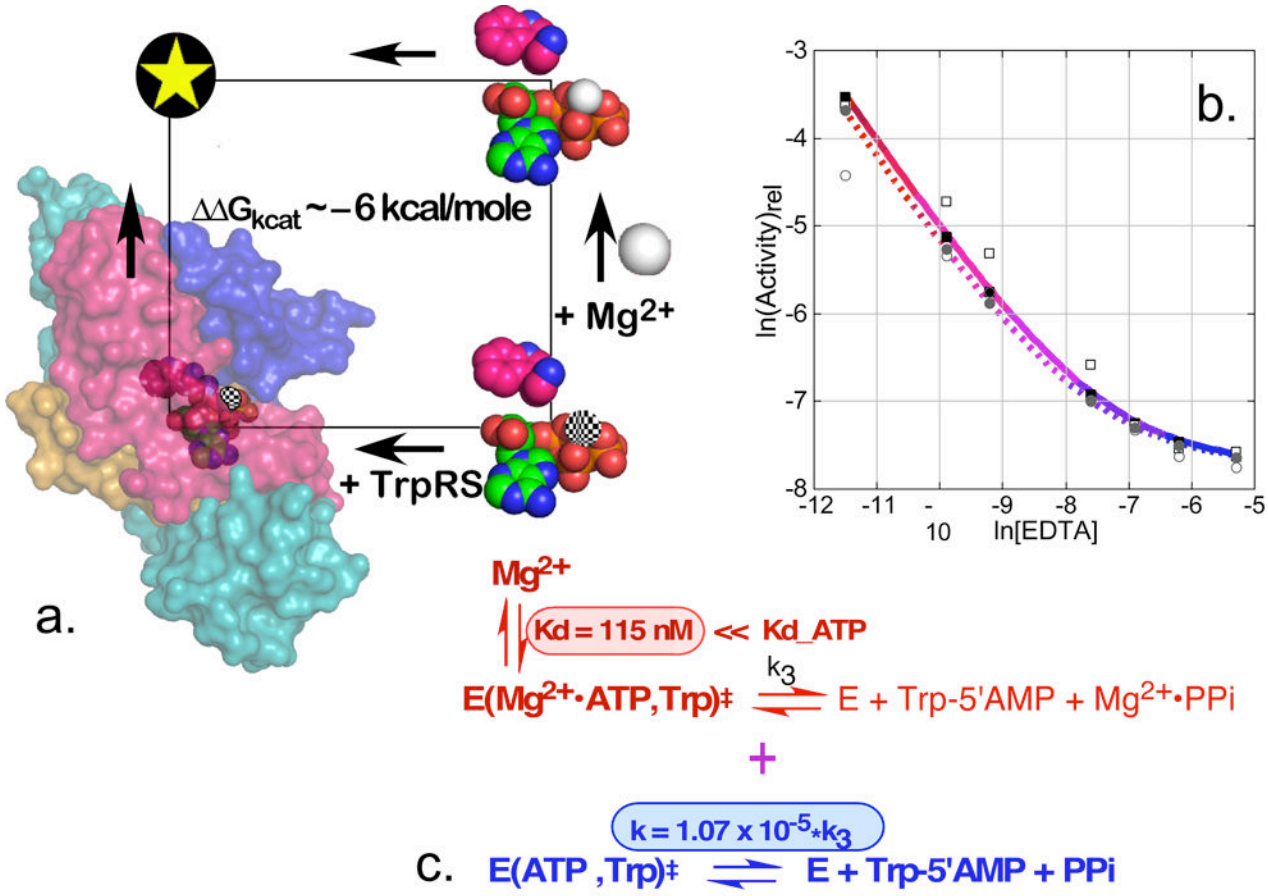

Figure 3.

The TrpRS•Mg^{2+} cycle (18). Native TrpRS is represented by a circled star. (*a*). Tryptophan activation is accelerated differently by TrpRS (10^9-fold), Mg^{2+} (fivefold), and their combination (10^{14}-fold), so $\Delta\Delta G_{int} \simeq -6.4$ kcal/mol. (*b*). Experimental data for the limiting rate acceleration in the absence of Mg^{2+}. Shown are catalytic assist by decreasing Mg^{2+} (*red*) and catalysis by metal-free TrpRS (*blue*). (*c*). Nonlinear fitting of the data shown in panel *b* yields $K_D^{\ddagger}$ for Mg^{2+} from the transition state (*red*) and the maximum rate acceleration by saturating Mg^{2+} concentrations (*blue*). Abbreviations: EDTA, ethylenediaminetetraacetic acid; PPi, pyrophosphate; TrpRS, tryptophanyl-tRNA synthetase. Figure adapted from References 20 and 108 with permission from AIP Publishing; copyright American Chemical Society.

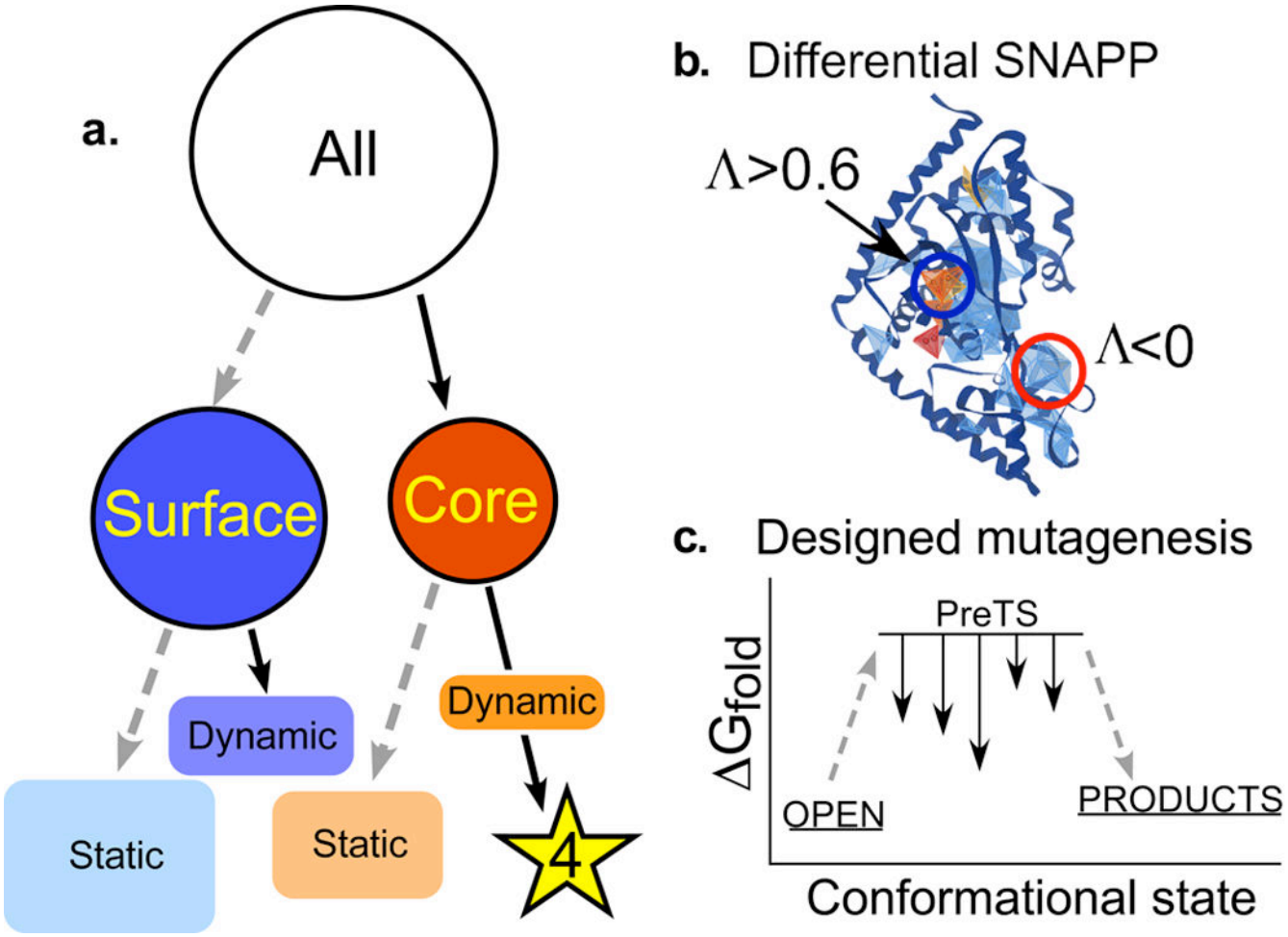

Figure 4.

Identifying molecular switches using geometric and energetic filters reduces the number of potential interactions involved in conformational transition states (18). (*a*) Parsing of interresidue contacts into dynamic/static and surface/core Delaunay simplices. (*b*) Geometric filtering by differential simplex identification and likelihood scoring. Compositions of dynamic simplices at the surface (*blue*) and in the core (*red*) change between conformations. (*c*) Energetic filtering. Vertical arrows indicate mutations that would stabilize the pretransition state, relative to open and products conformations. The star represents the four residues ultimately perturbed by combinatorial mutagenesis. Abbreviation: SNAPP, Simplicial Neighbor Analysis of Protein Packing. Figure adapted from Reference 20 with permission from AIP Publishing.

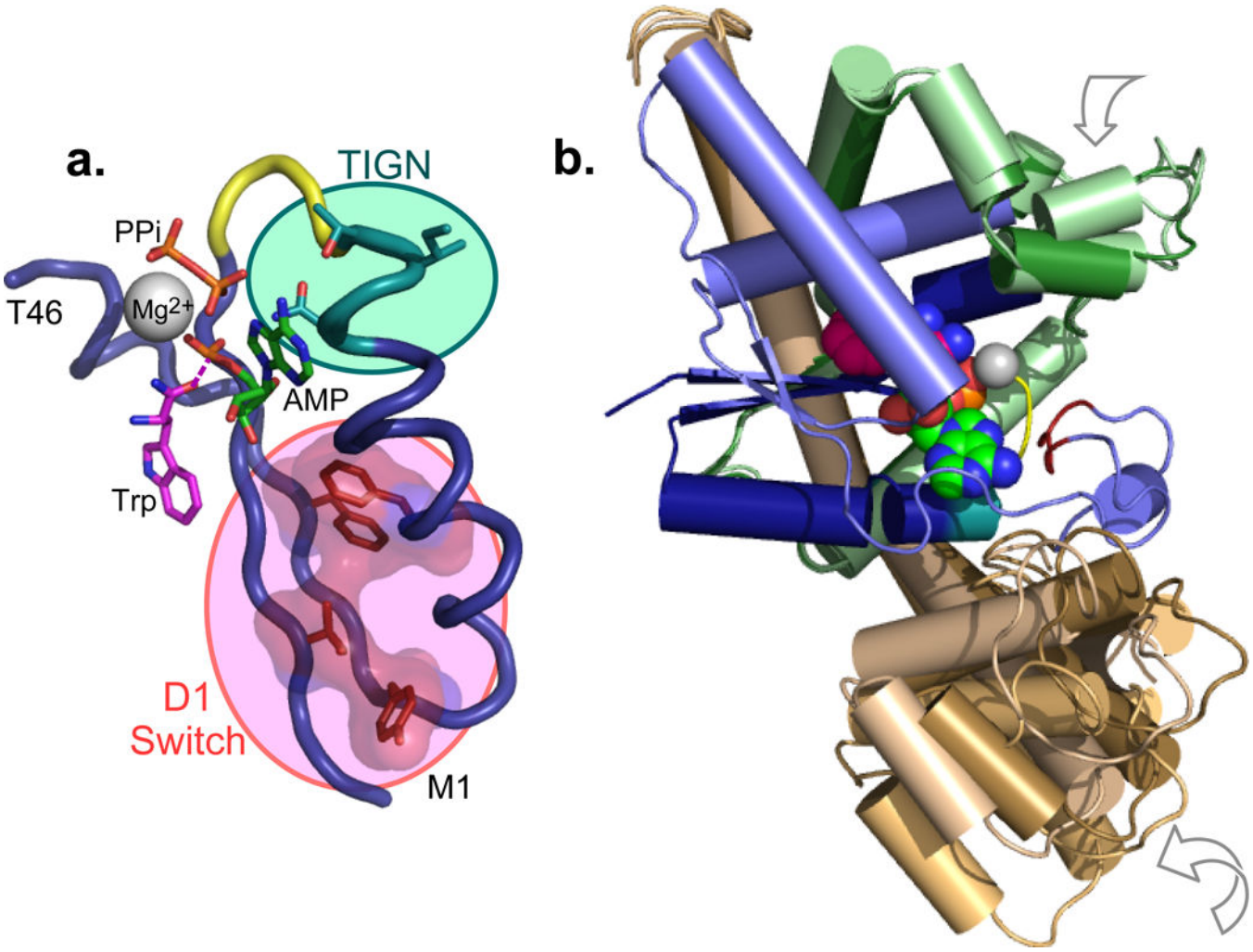

Figure 5.

Deconstruction of tryptophanyl-tRNA synthetase monomer (18). (*a*) The D1 switch is a tertiary packing domain present in >120 Rossmannoid superfamilies (14). Four residues mutated in this work are shown in red. The dark blue ribbon represents the protozyme (76) containing the D1 switch and catalytic TIGN (HIGH) signature (*teal*) at opposite ends of the α-helix. Tryptophan (*magenta*), ATP (*green*), and Mg^{2+} are shown as spheres. (*b*) Functional modules: protozyme (*dark blue*), Urzyme (*dark blue plus light blue* [**AU: Pls. distinguish by also describing relevant shapes**ED: I cannot come up with a graceful way to describe the relevant shapes. I hope that changing the way the colors of the Urzyme are stated, plus the identification of the N-terminal methionine in both A and B and repositioning these labels accomplishes what you seek here.]), connecting peptide 1 (CP1; *green*), and anticodon-binding domain (ABD; *amber*). Open/products CP1 and ABD configurations are indicated by gray curved arrows. Abbreviations: M1, the N-terminal methionine; PPi, pyrophosphate.

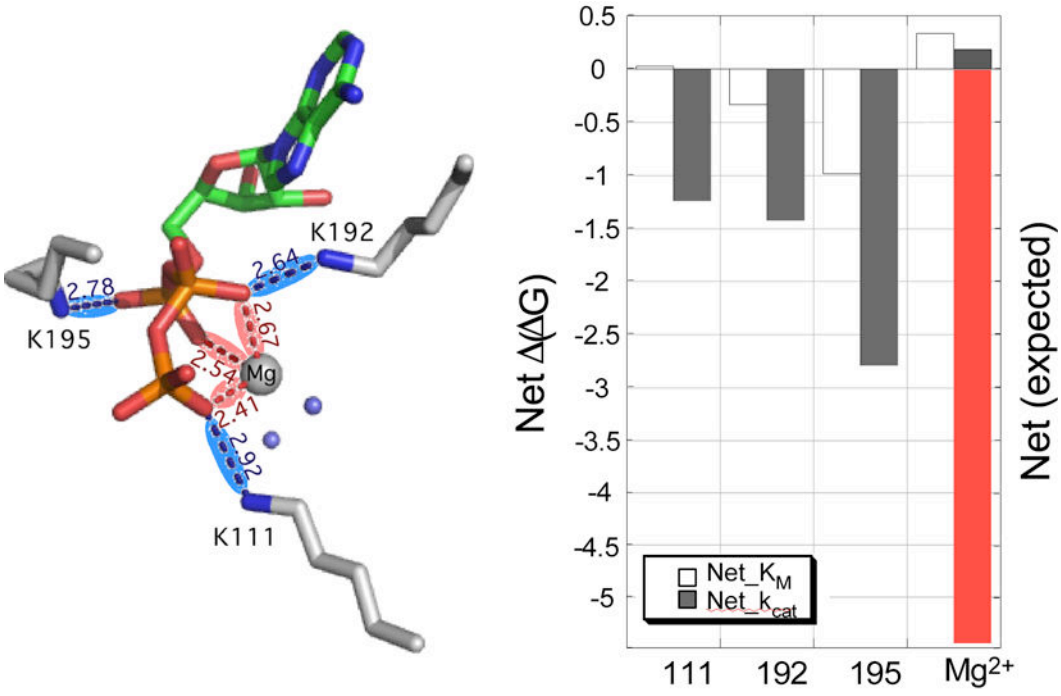

Figure 6.

Tryptophanyl-tRNA synthetase (TrpRS) does not coordinate Mg^{2+}, which is seen only in TrpRS pretransition state crystal structures (91), where it is coordinated only by ATP and water (70). Electrostatic competition for negative charges between Mg^{2+} and lysine residues weakens TrpRS affinity for ATP (64).

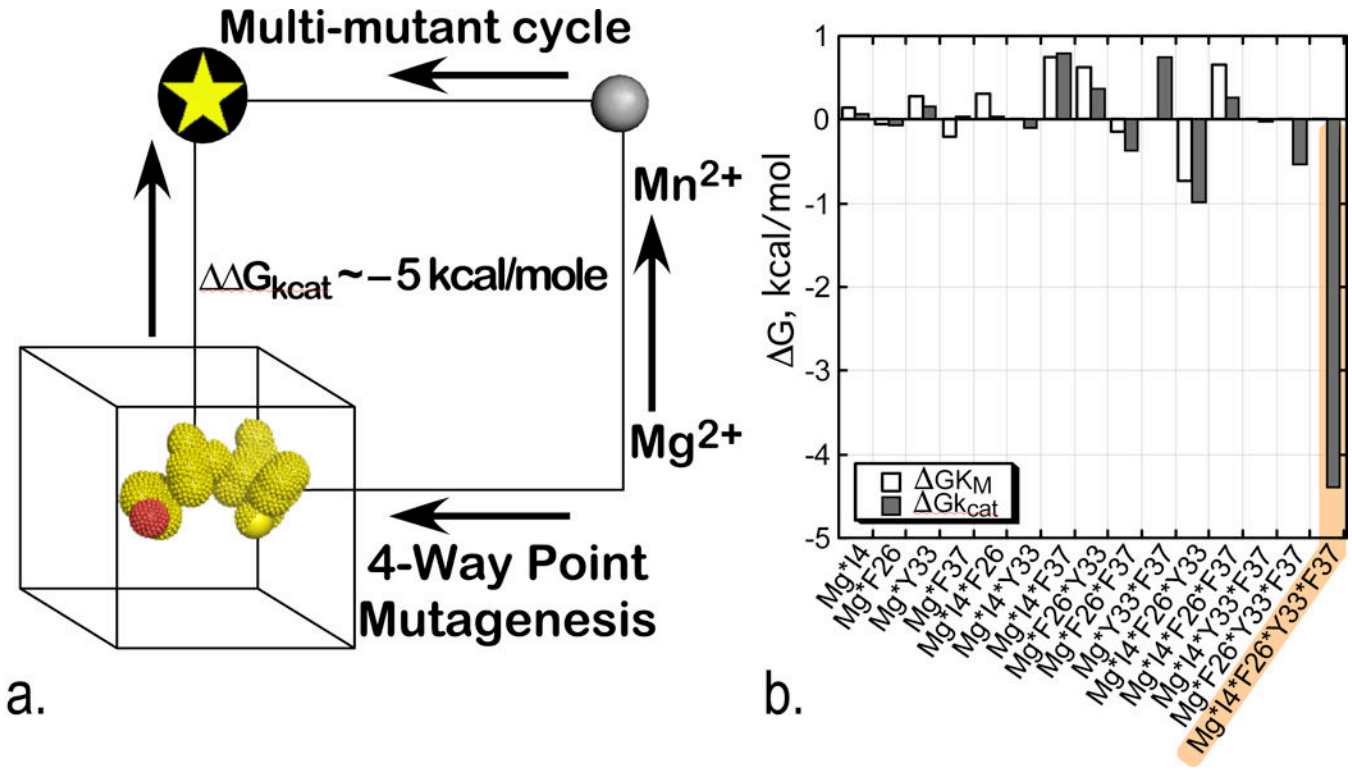

Figure 7.

Combinatorial mutagenesis of four D1 switch residues identifies a strong, five-way interaction (18, 109). (*a*) Schematic of the five-way thermodynamic cycle. (*b*) Combinatorial mutagenesis of I4, F26, Y33, and F37 and substitution of Mg^{2+} with Mn^{2+} reveal that all five moieties move coordinately in the chemical transition state. Native tryptophanyl-tRNA synthetase is represented by a circled star.

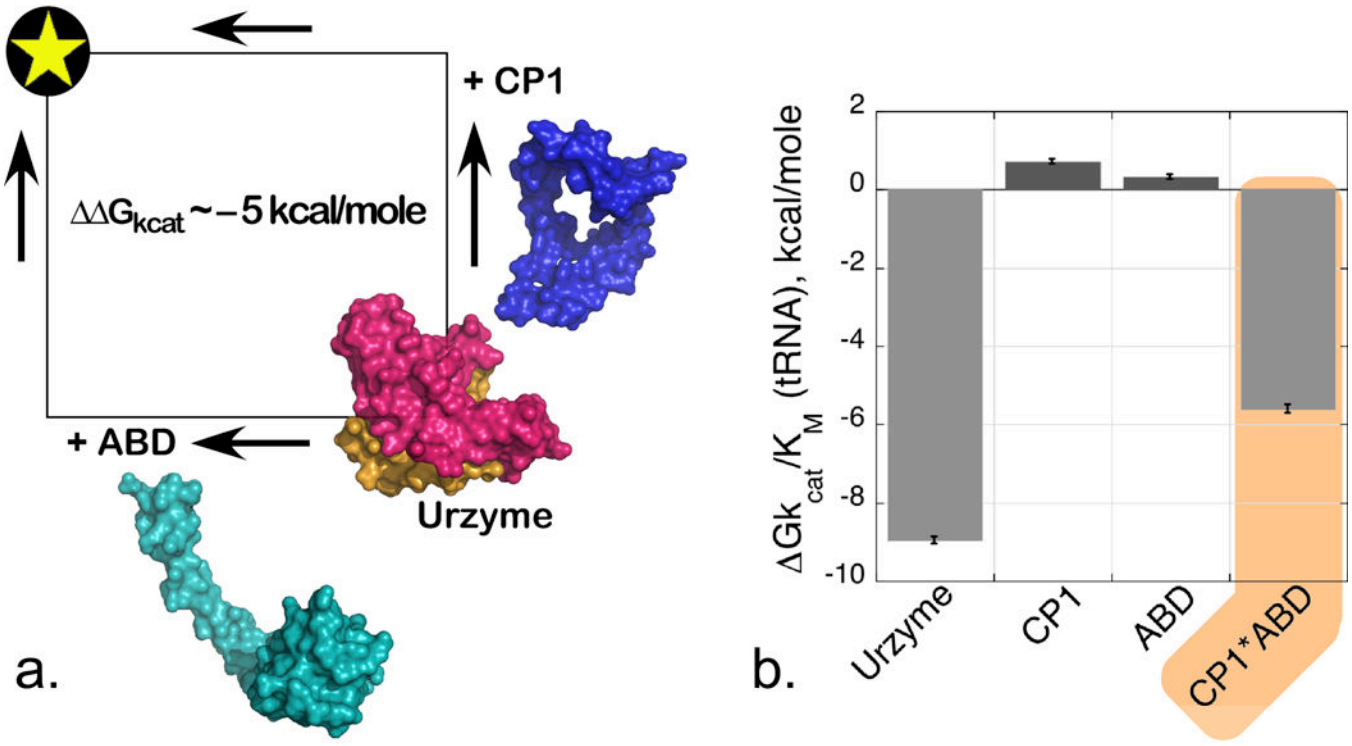

Figure 8.

Modular thermodynamic cycle (18, 67). (*a*) Schematic of the two-way modular variation. (*b*) Histogram of free energy contributions to ΔGk_{cat} for tRNA aminoacylation. Neither domain alone contributes favorably to catalysis; energetic coupling free energy is quantitatively equal to that for D1 switch•Mg^{2+} coupling. Native tryptophanyl-tRNA synthetase is represented by a circled star. Abbreviations: ABD, anticodon-binding domain; CP1, connecting peptide 1. Reproduced from Reference 20 with permission from AIP Publishing.

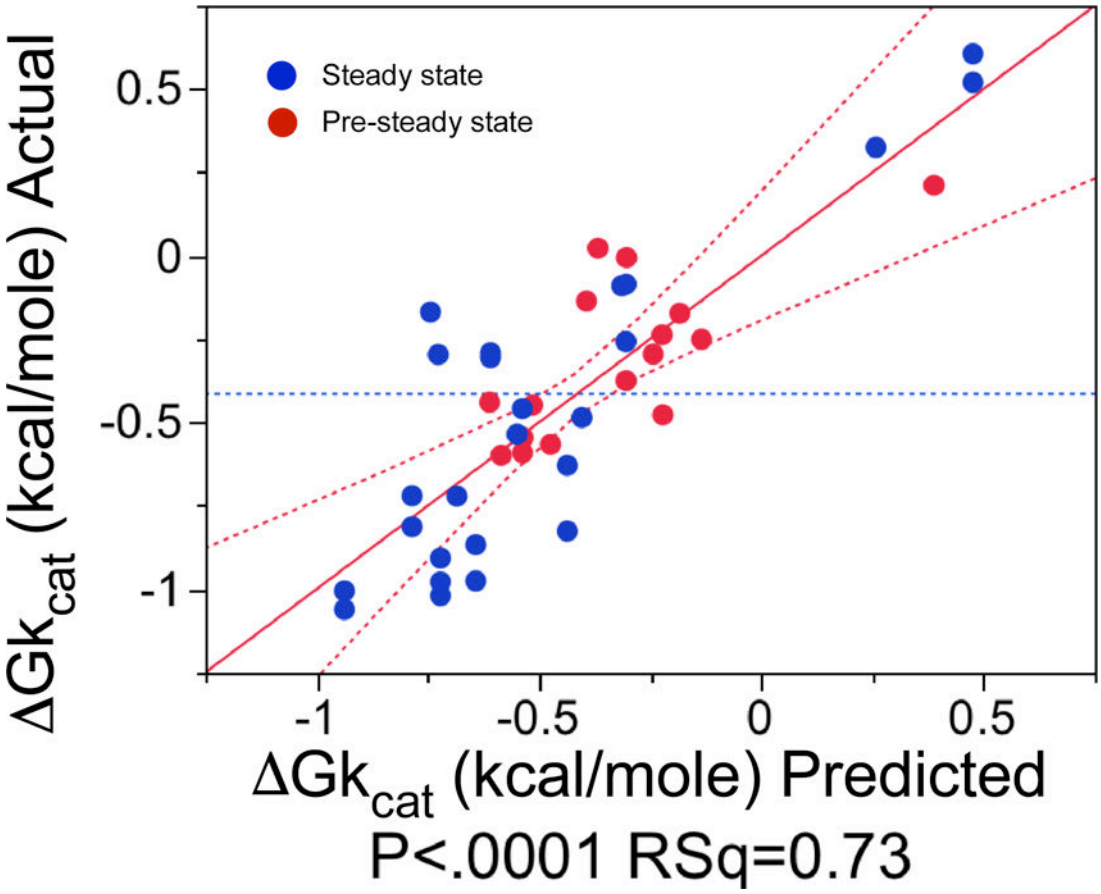

Figure 9.

Correlation between experimental rates for D1 switch variants and PATH parameters—Δ*G*, the energy difference between initial and final states; U_{trans}, the conformational barrier height; and the rates of forward and reverse reactions t_f and t_r—and their two-way interactions correlate with experimental rates for the 16 variants of the D1 switch. Steady-state (*blue*) and single-turnover (*red*) rates obey the same regression model. Figure adapted from Reference 20 with permission from AIP Publishing.